Available online at www.sciencedirect.com
SCIENCE DIRECT
Polymer 47 (2006) 4058–4067
polymer
www.elsevier.com/locate/polymer

Oxygen transport properties of liquid crystalline poly(pentamethylene 4,4′-bibenzoate)

Y.S. Hu, A. Hiltner *, E. Baer

Department of Macromolecular Science and Engineering, Center for Applied Polymer Research, Case Western Reserve University, Cleveland, OH 44106-7202, USA

Available online 20 March 2006

Abstract

This study examined the solid state structure and oxygen transport properties of smectic poly(pentamethylene 4,4′-bibenzoate) (PP5BB). The polymer was quenched from the isotropic melt to the smectic liquid crystalline (LC) glass and subsequently isothermally crystallized above the glass transition temperature. Crystallized PP5BB was characterized by thermal analysis and X-ray diffraction. Gas transport properties were characterized at 23 °C and 1 atm pressure. Examination of the smectic LC glass by atomic force microscopy (AFM) revealed a hierarchical structure in which mesogens organized into smectic layers, stacks of layers formed wavy lamellae, and assembles of lamellae defined domains. The effect of crystallization on the oxygen transport properties supported a simple two-phase model of impermeable crystallites dispersed in a permeable smectic glass. Due to the low-crystallite aspect ratio, crystallization only slightly increased the tortuosity of the diffusion pathway. This result provided the structural basis for describing oxygen permeability in terms of the Nielsen model for low-aspect ratio particles. The hierarchical LC structure of PP5BB closely resembled that reported for poly(diethylene glycol 4,4′-bibenzoate) (PDEGBB), which has the same chemical structure as PP5BB except that the center methylene of the spacer is replaced with an ether oxygen. However, oxygen permeability of PP5BB was about three times higher than that of PDEGBB. Non-LC aromatic polyesters with pentamethylene diol spacers also had oxygen permeability about three times higher than the corresponding polyester with diethylene glycol spacers due primarily to higher diffusivity. The effect was traced to differences in the sub-ambient mechanical relaxation behavior.

Keywords: Liquid crystalline polymer; Oxygen transport; Polyesters

1. Introduction

Aromatic liquid crystalline polymers (LCPs) stand out as having remarkably low gas permeability compared to most thermoplastics. The extraordinarily low gas permeability of LCPs stems mainly from low solubility rather than from low diffusivity [1–5]. The complex phase transitions and morphologies typical of LCPs present a particular challenge to structural modeling of gas transport. In recent studies, the challenges were addressed with an LCP from the family of smectic polyesters based on 4,4′-bibenzoic acid, poly(diethylene glycol 4,4′-bibenzoate) (PDEGBB) [6–8]. A hierarchical structural model provided the basis for understanding the excellent oxygen barrier of PDEGBB and revealed a glassy LC state with hole free volume intermediate between those of the permeable amorphous glass and the impermeable three-dimensional crystal. In this interpretation, LC order leads to inherently low gas solubility.

Crystallization of the smectic PDEGBB glass reduced gas permeability further, primarily by reducing solubility. The linear decrease in oxygen solubility with crystallinity conformed to the simple two-phase gas transport model that has been exceptionally useful for describing the effect of crystallization on oxygen transport of non-LC aromatic polyesters [9–11]. For PDEGBB, the low-aspect ratio of the small crystals imparted much less tortuosity to the diffusion pathway than is typical of non-LC lamellar crystals. The concept of small impermeable crystals dispersed in a permeable glassy LC matrix lead to application of the generalized Maxwell equation for permeability [6].

The present study examines how replacing the ether oxygen in the PDEGBB spacer with a methylene group affects the solid state structure and the oxygen transport properties. Poly (pentamethylene 4,4′-bibenzoate) (PP5BB) is a well-characterized smectic LCP [12–14]. Like PDEGBB, PP5BB forms a crystallizable smectic LC glass. In addition, this study compares the oxygen transport properties of PDEGBB and PP5BB with some non-LC aromatic polyesters having diethylene glycol and pentamethylene diol spaces.

* Corresponding author.
E-mail address: pah6@case.edu (A. Hiltner).

0032-3861/$ - see front matter © 2006 Elsevier Ltd. All rights reserved.
doi:10.1016/j.polymer.2006.02.033

2. Materials and methods

Poly(pentamethylene 4,4′-bibenzoate) (PP5BB) was provided by KoSa (Spartanburg, SC) in the form of extruded pellets. The chemical structure of PP5BB is:

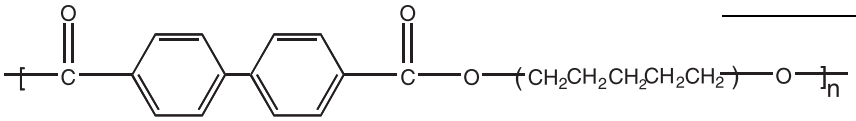

The intrinsic viscosity of the PP5BB pellets was 0.76 dl g^{-1}, measured at 25 °C in 1% (w/w) dichloroacetic acid solution. Poly(pentamethylene naphthalate) (PP5N), poly(diethylene glycol naphthalate) (PDEGN), poly(pentamethylene 4,4′-bibenzoate-*co*-isophthalate) with 30 mol% isophthalate (PP5BB-30I), and poly(diethylene glycol 4,4′-bibenzoate-*co*-isophthalate) with 30 mol% isophthalate (PDEGBB-30I) were also provided by KoSa with intrinsic viscosity of 0.75, 0.64, 0.77, and 0.66 dl g^{-1}, respectively, measured according to the method described for PP5BB.

The pellets were dried in vacuo at 50 °C for 24 h prior to molding. Films 180–200 μm thick were obtained by compression molding the pellets between Kapton® sheets in a press at 250 °C, which was 40 °C above the clearing point of PP5BB. The platens were heated in the press for 3 min with repeated application and release of pressure to remove air bubbles, and held at 309 psi (2.1 MPa) for an additional 3 min. The polymer could not be quenched to the amorphous glass due to the extremely rapid isotropic to liquid crystalline transition. Quenched LC films were obtained by plunging the isotropic melt into ice water. Some of the quenched films were subsequently annealed at 105 or 160 °C for a period of time and quenched in ice water. The annealed films are identified as A105 or A160 followed by the annealing time, Table 1. Slowly cooled films, identified as SC165, were cooled in the press at approximately 2 °C min^{-1} from 250 to 165 °C and quenched into ice water.

Density was measured at 23 °C with a density gradient column constructed from an aqueous solution of calcium nitrate in accordance with ASTM-D 1505 Method B. The column was calibrated with glass floats of known density. Small pieces of film ($\sim$25 mm^2) were placed in the column and allowed to equilibrate for 30 min before the measurements were taken.

Thermal analysis was conducted with a Perkin–Elmer DSC-7 calibrated with indium and tin under nitrogen. Heating and cooling scans were performed at 10 °C min^{-1} over the temperature range from 0 to 280 °C.

Relaxation behavior was measured in a dynamic mechanical thermal analyzer (DMTA) Mk II unit from Polymer Laboratories (Amherst, MA) operated in the tensile mode with a frequency of 1 Hz and heating rate of 3 °C min^{-1}.

Wide angle X-ray diffraction (WAXD) patterns were obtained at ambient temperature with a Philips diffractometer in the transmission mode using a slit angle of 1/12°.

Positron annihilation lifetime spectroscopy (PALS) was performed using a conventional fast–fast coincidence system. The instrumentation and procedures for data analysis were described previously [15].

Conformational composition was determined by photoacoustic Fourier transform infrared (FTIR) spectroscopy. Spectra were collected at ambient temperature with a Nicolet 870 FTIR spectrometer using a MTEC Model 200 photoacoustic cell. Specimens were cut from the molded films and dried overnight in vacuo at ambient temperature to remove moisture. The peaks at 960 cm^{-1} (trans) and 898 cm^{-1} (gauche) were used for conformational analysis. The peak

Table 1
Oxygen barrier properties of PP5BB

Sample	Density (g cm^{-3})	P (cc(STP) cm m^{-2} atm^{-1} day^{-1})[a]	D (10^{-13} m^2 sec^{-1})	S (cc(STP) cm^{-3} atm^{-1})	(ΔH_{X-S}) (J g^{-1})	Trans fraction	ϕ_c
Quenched	1.2623±0.0012	0.0921±0.0008	6.5±0.1	0.0164±0.0004	0	0.72	–
A 105-4 min	1.2697±0.0009	0.0686±0.0007	5.4±0.1	0.0147±0.0002	8.0±0.2	0.77	0.11
A 105-10 min	1.2719±0.0006	0.0661±0.0007	5.3±0.1	0.0144±0.0001	10.3±0.2	–	0.14
A 105-15 min	1.2727±0.0008	0.0647±0.0001	5.2±0.1	0.0144±0.0001	11.2±0.1	0.81	0.15
A 105-30 min	1.2750±0.0008	0.0619±0.0008	5.2±0.1	0.0138±0.0003	13.5±0.8	–	0.18
A 105-1 h	1.2762±0.0009	0.0610±0.0010	5.1±0.1	0.0138±0.0004	15.0±0.2	–	0.20
A 105-4 h	1.2771±0.0002	0.0591±0.0002	5.2±0.1	0.0132±0.0001	15.4±0.2	–	0.21
A 105–10 h	1.2775±0.0008	0.0577±0.0002	5.1±0.1	0.0131±0.0004	16.7±0.4	0.82	0.22
A 105-24 h	1.2779±0.0003	Brittle	–	–	17.5±0.5	0.83	0.22
A 160-0.5 min	1.2699±0.0002	0.0660±0.0006	5.5±0.1	0.0139±0.0003	9.5±0.2	–	0.11
A 160-1 min	1.2729±0.0002	0.0600±0.0005	5.3±0.1	0.0131±0.0003	11.2±0.2	0.80	0.15
A 160-2 min	1.2742±0.0004	0.0539±0.0010	5.1±0.1	0.0122±0.0008	12.4±0.5	0.80	0.17
A 160-4 min	1.2767±0.0003	0.0514±0.0008	5.0±0.1	0.0119±0.0006	15.3±0.1	–	0.21
A 160-10 min	1.2778±0.0005	Brittle	–	–	16.5±0.4	–	0.23
A 160-4 h	1.2786±0.0002	Brittle	–	–	18.6±0.2	0.82	0.24
A 160-12 h	1.2800±0.0002	Brittle	–	–	19.0±0.1	0.84	0.26
SC 165	1.2635±0.0010	0.0796±0.0004	6.3±0.1	0.0146±0.0003	0	0.81	–

[a] 0.152 Barrers.

heights were normalized to the carbonyl stretching band at 1730 cm^{-1}. Detailed determination of the fraction of trans conformations is described elsewhere [16].

Free surfaces were prepared for atomic force microscopy (AFM). Small pieces of the pellet were sandwiched between clean glass cover slides, heated into the isotropic state (about 230 °C) on the hot stage of an optical microscope and lightly pressed to spread out the melted polymer. After the specimen was removed from the hot stage and cooled to ambient temperature, one of the cover slides was peeled off to create a free surface. The specimen with the free surface was vacuum dried, re-melted under nitrogen, and subjected to a thermal history that mimicked the compression molded films, i.e. quenched, annealed or slowly cooled. Sometimes the free surfaces were etched for 6 h with 40 wt% aqueous methylamine solution at 23 °C using the procedures of Organ et al. [17]. The etched specimens were washed with de-ionized water and methanol. Initially the specimens were about 35–50 μm in thickness. Etching removed material from the surface to a depth of about 100–200 nm. The surfaces were examined by AFM; the images were obtained in air at ambient conditions using the Nanoscope IIIa MultiMode head from Digital Instruments (Santa Barbara, CA). Experiments were conducted in the tapping mode using Si probes with 50 N m^{-1} spring constant and resonance frequencies in the range 284–362 kHz. The tip had a radius of 10 nm. Height and phase images were recorded simultaneously.

Oxygen flux $J(t)$ at 0% relative humidity, 1 atm pressure, and 23 °C was measured with a MOCON OX-TRAN 2/20. Specimens were carefully conditioned as described previously in order to obtain the non-steady-state oxygen flux from which the diffusivity D was determined [9]. To obtain the diffusivity D and to accurately determine the permeability P, the data were fit to the solution of Fick's second law with appropriate boundary conditions [9]

$$J(t) = \frac{Pp}{l}\left[1 + 2\sum_{n=1}^{\infty}(-1)^n \exp\left(-\frac{D\pi^2 n^2 t}{l^2}\right)\right] \quad (1)$$

where p is the oxygen pressure and t is the time. As indicated previously, the error in determining the two fitting parameters, P/l and D/l^2, was estimated not to exceed 2% [9]. The average thickness l of each specimen was determined as $l = W(A\rho)^{-1}$, where W is the sample weight, A is the sample area and ρ is the density. All the samples were stored in the freezer and all the analyses were accomplished within 4 weeks of preparation in order to avoid possible aging effects.

3. Results and discussion

3.1. Thermal transitions

The thermograms in Fig. 1 were obtained by cooling PP5BB from 280 to 0 °C at a rate of 10 °C min^{-1} and subsequently heating it at the same rate. The cooling curve contained two exothermic peaks at 197 and 87 °C, corresponding to the isotropic-to-smectic transition (I–S) and the smectic-to-crystalline (S–X) transition, respectively [18]. The heating curve showed a weak glass transition at 32 °C. A broad exothermic cold crystallization peak at 80–150 °C before the endothermic crystalline-to-smectic (X–S) transition at 174 °C indicated that the smectic polymer did not completely crystallize during cooling at 10 °C min^{-1}. The smectic-to-isotropic (S–I) transition occurred at 209 °C, close to the temperature of the I–S transition in the cooling curve.

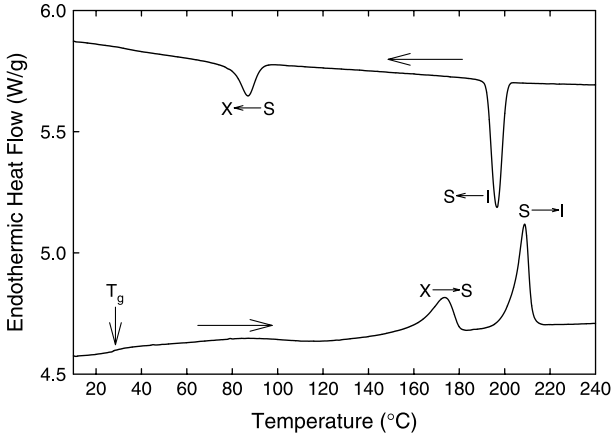

Fig. 1. Thermograms of PP5BB cooled from the isotropic melt to the LC glass and reheated at 10 °C min^{-1}.

The heating thermograms of compression-molded PP5BB films are shown in Fig. 2. The quenched film exhibited a distinct glass transition at 30 °C, a very broad cold crystallization peak in the temperature range 80–150 °C, followed by the X–S and S–I transitions at the same temperatures as in Fig. 1. An absolute enthalpy of about 11.0 J g^{-1} for both cold crystallization and subsequent melting categorized the quenched PP5BB film as an LC glass without conventional crystallinity. The heating thermogram of PP5BB that had been slowly cooled from the isotropic melt through the I–S transition to 165 °C and then quenched was the same as the heating thermogram of the quenched film, although the density increased slightly from 1.2623 g cm^{-3} for quenched PP5BB to 1.2635 g cm^{-1} suggesting that slow-cooling produced an LC glass with somewhat better order than quenching directly from the isotropic melt.

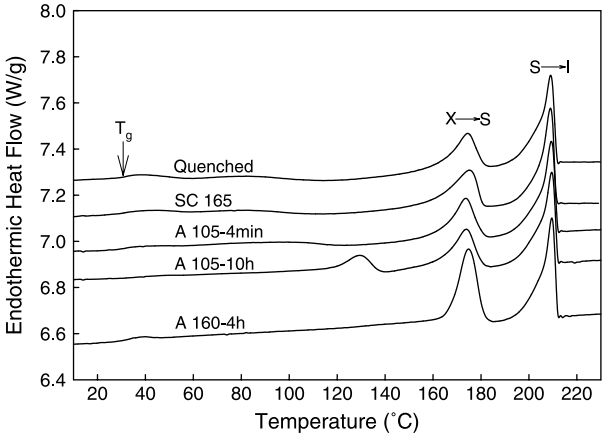

Fig. 2. Heating thermograms of PP5BB with various thermal histories.

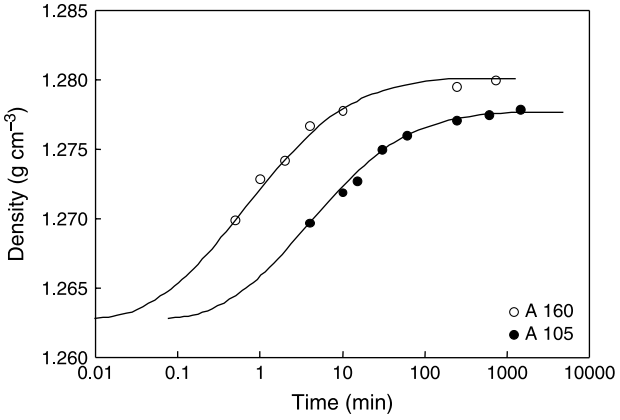

Fig. 3. Crystallinity measured as density as a function of annealing time after quenching.

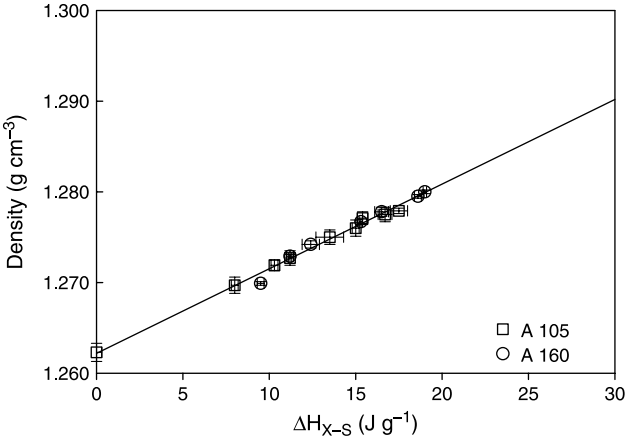

Fig. 4. Relationship between density and crystallinity measured as ΔH_{X-S}, the sum of the exothermic heat of cold crystallization and the endothermic heat of the X–S transition.

Annealing quenched PP5BB at 105 °C for 4 min reduced the enthalpy of cold crystallization, Fig. 2. A longer annealing time of 10 h produced a new endothermic peak at about 130 °C, associated with imperfect crystals developed at the relatively low crystallization temperature. A higher annealing temperature of 160 °C resulted in a single strong melting endotherm. The enthalpy of the X–S transition (ΔH_{X-S}) was 17.5 J g^{-1} after crystallization at 105 °C for 24 h and 19.0 J g^{-1} after crystallization at 160 °C for 12 h. Such a low value of ΔH_{X-S} seems to be characteristic of the X–S transition for LC poly(bibenzoates) with an odd number of carbon atoms in the spacer backbone [19,20]. Regardless of the thermal history, the enthalpy of the S–I transition (ΔH_{S-I}) was 17.4 J g^{-1}.

An increase in density and an increase in fraction of trans conformations accompanied crystallization, Table 1. The increase in crystallinity expressed as the density of annealed PP5BB films followed the typical sigmoidal dependence on isothermal crystallization time as shown in Fig. 3. Increasing the isothermal crystallization temperature resulted in faster crystallization and slightly higher plateau density. Increasing density correlated with increasing crystallinity from DSC (ΔH_{X-S}) measured as the sum of the exothermic heat of cold crystallization and the endothermic heat of melting. The relationship between density and ΔH_{X-S} is plotted in Fig. 4. Data for both crystallization temperatures defined a single linear relationship.

3.2. Wide angle X-ray diffraction

It has been demonstrated that PP5BB belongs to the smectic CA family, where the smectic layer normal is parallel to the molecular chain direction and the mesogenic groups are tilted with respect to the molecular chain direction [21,22]. The WAXD pattern of quenched films in Fig. 5 exhibited a sharp peak at $2\theta = 5.75°$ and its second order, corresponding to a smectic layer spacing of 15.4 Å. The observed spacing was in agreement with the literature report and was less than the calculated length of the fully extended repeat unit of 17.2 Å [21]. Infrared analysis of the chain configuration provided corroboration that the spacer was not fully extended in PP5BB. The trans fraction was found to be 0.72, which allowed for a significant fraction of non-trans conformations. The broad reflection in the WAXD pattern centered at 20.5° (4.33 Å) was attributed to lateral packing of the mesogens. Slowly cooling to 165 °C before quenching did not alter the diffraction pattern.

Crystallization at 105 °C produced additional broad reflections superimposed on the peak at 20.5° indicating some amount of three-dimensional crystalline order, Fig. 5. Crystallization at 160 °C generated stronger reflections and additional peaks with the strongest reflections at 2θ values of 18.3, 21.0, 21.3, 22.5 and 25.3°. Despite the increase in crystalline order, there was only a small shift in the layer reflection from 5.75 to 5.80° (15.4–15.2 Å) for the PP5BB film with the highest crystallinity.

The crystal structure has been indexed for PP5BB fiber spun from the isotropic melt and subsequently annealed at about 180 °C [23]. It was reported that PP5BB took the monoclinic lattice with $a = 5.84$ Å, $b = 5.10$ Å, $c = 30.0$ Å (chain axis) and $\gamma = 56.0°$. Two repeat units were included in the c-dimension. The strongest crystalline reflections were located at 2θ values of 18.3, 21.0, 21.3, and 21.5°. The results for PP5BB film annealed at 160 °C were consistent with the reported reflections

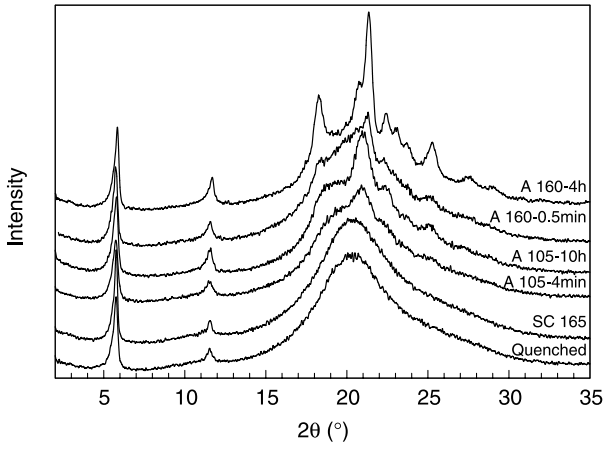

Fig. 5. WAXD scans of PP5BB films with various thermal histories.

assuming that the two reflections at 21.3 and 21.5° were merged into a single peak at 21.3°.

3.3. Dynamic mechanical relaxation behavior

Representative DMTA scans of PP5BB films in Fig. 6 show storage modulus (E') and loss tangent (tan δ) as a function of temperature. The β-relaxation corresponded to the glass transition [6]. The peak temperature of 41 °C for the quenched LC glass was in agreement with literature reports [19]. The peak tan δ value of about 0.43 for the quenched LC glass was only about one fourth the intensity of the tan δ peak for the glass transition of a typical non-LC glassy polyester. The accompanying drop in E' of 1.5 orders of magnitude was correspondingly less than the drop of 3–4 orders of magnitude observed with a non-LC polyester glass. Slowly cooling PP5BB through the I–S transition before quenching produced only a slight decrease in tan δ peak intensity from 0.43 to 0.33 without affecting peak temperature, which suggested that the nature of the LC glass remained largely unchanged. In contrast, crystallization reduced the β-relaxation intensity considerably, broadened the peak and increased the transition temperature. The accompanying drop in E' was correspondingly smaller. These effects followed trends that are typical for crystallization of a non-LC polyester glass.

The broad γ-relaxation from −150 to −30 °C is characteristic of aromatic polyesters with flexible spacers [6]. The γ-relaxation region of PP5BB showed two distinct peaks. For convenience they are identified as γ_1 at higher temperature and γ_2 at lower temperature. For PP5BB, crystallization decreased the γ_1 intensity without affecting the γ_2 intensity or the peak temperatures.

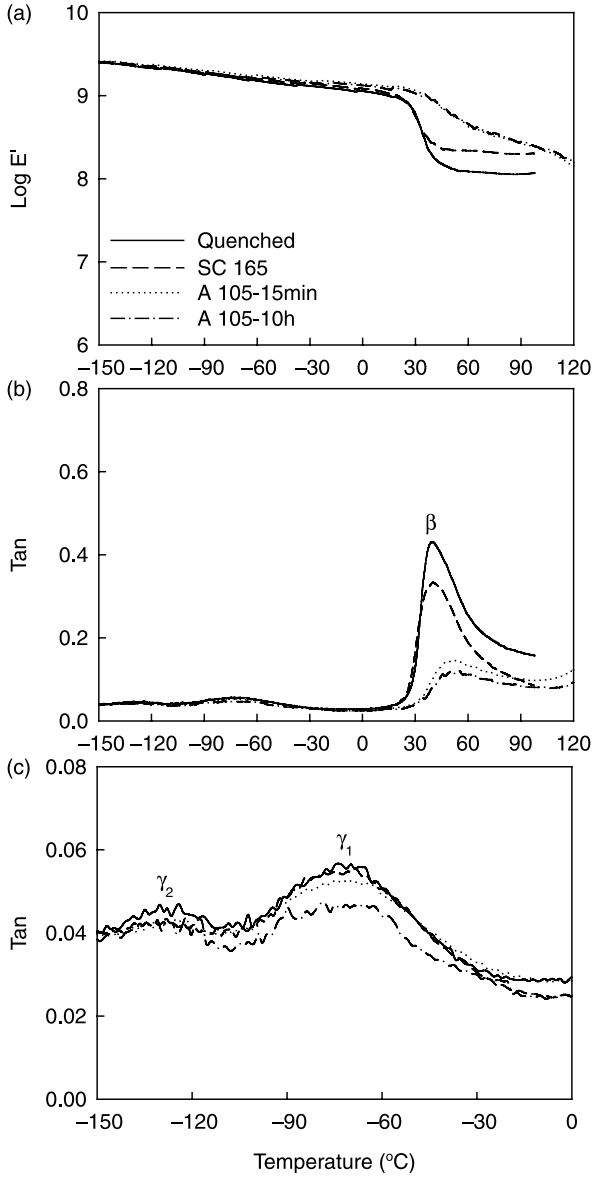

Fig. 6. DMTA curves of quenched, slowly cooled, and annealed PP5BB: (a) log E'; (b) tan δ, (c) low temperature range of tan δ.

3.4. Morphology

The morphology of the LC glass that had been slowly cooled through the I–S transition to 165 °C and quenched displayed a polygonal texture with domains on the 1 μm size scale, Fig. 7(a). Etching selectively removed the domain boundaries, making the domains clearer, Fig. 7(b). The domains consisted of arrays of short lamellae with thickness of 50 nm. The morphology of slowly cooled PP5BB was in accordance with previous descriptions of PDEGBB [6].

Quenching through the I–S transition prevented formation of well-defined polygonal domains on the surface of PP5BB. However, etching revealed the irregular boundaries of small, poorly defined domains on the size scale of 200–300 nm, Fig. 8(a). Occasionally, individual lamellae were discernable in the 1-μm phase image (arrows). With thickness of about 15–18 nm, the lamellae were much thinner than the lamellae in slowly cooled films. The poorly defined domain texture remained after quenched PP5BB was crystallized at 105 °C, Fig. 8(b). The thin lamellae within the domains were more distinct than in the quenched film (arrows), however, the lamellar thickness did not change. In contrast, crystallization of quenched PP5BB at 160 °C for only 3 min produced a well-defined lamellar morphology with lamellar thickness of 20–24 nm, as shown in the 3-μm phase image Fig. 8(c). After 6 min at 160 °C, the lamellar thickness increased slightly

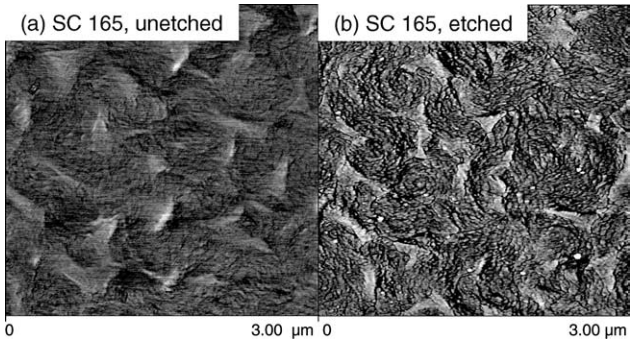

Fig. 7. AFM phase images of slowly cooled PP5BB: (a) before etching and (b) after etching.

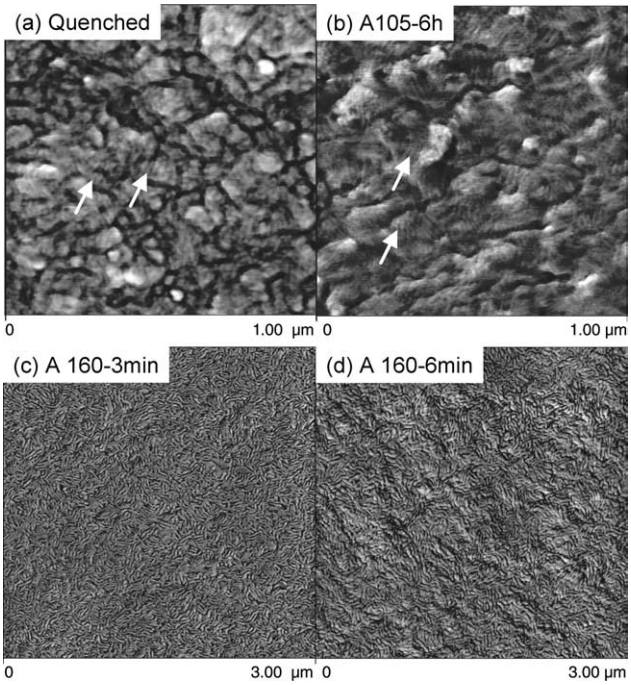

Fig. 8. AFM phase images of quenched PP5BB: (a) etched; (b) annealed for 24 h at 105 °C, etched; (c) annealed at 160 °C for 3 min, unetched and (d) annealed at 160 °C for 6 min, unetched.

to 22–26 nm, Fig. 8(d). However, annealing did not produce the well-defined domain morphology seen in slowly cooled films (compare Fig. 8(d) with Fig. 7(b)).

3.5. Structural model

A hierarchical structural model is proposed for PP5BB based on the combined results of AFM and WAXD. The model closely resembles that proposed for PDEGBB [6]. More or less extended chains assemble with the mesogens organized into smectic layers. From WAXD [21], the smectic layers are oriented perpendicular to the chain axis and individual mesogens within the smectic layer are tilted at a slight angle to the chain direction. The spacing of the smectic layers is 1.54 nm from WAXD, which is less than the extended chain dimension, estimated at 1.72 nm [21]. This may be a general feature of smectic LCPs, and indicates some gauche kinks or eclipsed conformations. Stacks of smectic layers form lamellae. Regular stacking of the smectic layers is periodically interrupted by disordered regions that contain chain ends, chain folds, and other chain defects. These interruptions define the thickness of the lamellae, which ranges from 15 nm in quenched films to 50 nm in slowly cooled films. The lamellae often exhibit a granular texture that suggests some lateral variation in order within the regular stacking. Assemblies of lamellae define domains on the micron size scale.

Crystallization of PP5BB at relatively low temperature (105 °C) does not produce the lamellar or spherulitic features that are characteristic of non-LC aromatic polyesters [24]. It is a general observation that crystallization from the LC state retains the texture of the LC precursor [6]. Following previous studies of semicrystalline smectic LCPs, the structural image of crystallized PP5BB consists of small fringed micellar crystals imbedded in a smectic mesophase [25,26]. The mesophase is not significantly disrupted by crystallization [27,28]. Reports of a crystalline long spacing of 10–20 nm in other poly(bibenzoates) [29], a dimension which is similar to the LC lamellar thickness, supports the general picture of small embedded crystallites. Annealing at a higher temperature (160 °C) causes rapid reorganization of the smectic phase to more highly organized and thicker lamellae. Simultaneous crystallization produces crystallites imbedded in the smectic lamellae.

3.6. Oxygen transport

Typical experimental curves in Fig. 9 describe the oxygen flux $J(t)$ through quenched, slow-cooled and crystallized PP5BB films. To facilitate comparisons among specimens that varied somewhat in thickness, the flux curves were normalized to a film thickness of 200 μm using transport parameters determined from the original film thickness. Careful conditioning and appropriate choice of specimen thickness resulted in excellent resolution of the various features of the time dependence. The initial increase in oxygen flux reflected non-steady-state diffusion. This part of the curve was controlled mainly by the diffusivity D. As the permeant concentration in the specimen reached a constant distribution, the flux reached the steady-state value J_0. This value, normalized to the film thickness l and the permeant gas pressure p, defined the permeability $P = J_0 l p^{-1}$.

Compared to quenching, slow-cooling did not affect the non-steady-state region of the flux curve, whereas the steady-state flux decreased slightly (lower permeability). Crystallization of the quenched LC glass affected both the non-steady-state and steady-state parts of the flux curve. The non-steady-state region broadened slightly (lower diffusivity) and the steady-state flux decreased significantly. The fit to the solution of Fick's second law (Eq. (1)) is included with the experimental points in Fig. 9. The fit was equally good for all the experiments in the study. The two fitting parameters, P/l and D/l^2, were used to obtain

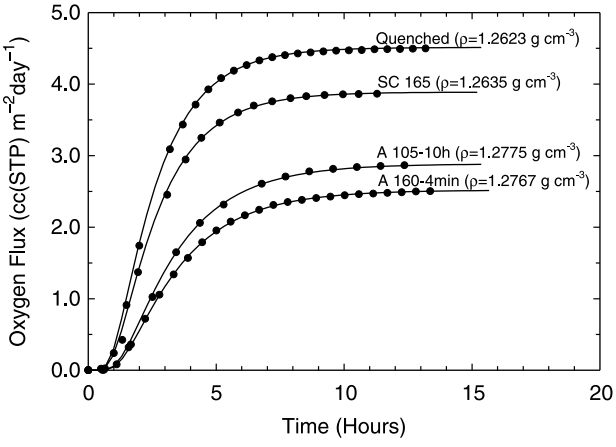

Fig. 9. Experimental $J(t)$ data for PP5BB films and the fit to Eq. (1).

Table 2
Oxygen barrier properties of selected polyesters

Sample	Density (g cm^{-3})	T_g (°C)	P (cc(STP) cm m^{-2} atm^{-1} day^{-1})[a]	D (10^{-13} m^2 sec^{-1})	S (cc(STP) cm^{-3} atm^{-1})	Free volume hole radius (Å)	Trans fraction
PET	1.3370	76	0.450	5.8	0.090	2.56	
Quenched PP5BB	1.2623	30	0.0921±0.0008	6.5±0.1	0.0164±0.0004	2.34	0.72
Quenched PDEGBB	1.3201	42	0.0318±0.0004	2.6±0.1	0.0142±0.0002	2.23	0.79
SC PP5BB	1.2635	30	0.0796±0.0004	6.3±0.1	0.0146±0.0003	2.36	
SC PDEGBB	1.3309	42	0.0267±0.0004	2.7±0.1	0.0114±0.0003	2.21	
PP5N	1.2549	46	0.202±0.001	4.8±0.1	0.0489±0.0004	2.36	
PDEGN	1.3131	55	0.0777±0.0018	1.7±0.1	0.0533±0.0008	2.41	
PP5BB-30I	1.2426	28	0.314±0.009	10.3±0.3	0.0352±0.0010	–	0.67
PDEGBB-30I	1.3060	34	0.110±0.002	3.6±0.1	0.0354±0.0008	2.40	0.71

[a] 0.152 Barrers.

diffusivity D and to accurately determine the permeability P. Solubility S was calculated from the relationship $S=PD^{-1}$.

Quenched PP5BB had oxygen permeability about five times lower than that of amorphous poly(ethylene terephthalate) (PET), Table 2. The low oxygen permeability of PP5BB resulted mainly from low gas solubility. To better assess the effect of liquid crystallinity on oxygen transport characteristics, comparisons were made with a glassy non-LC polyester having about the same T_g as PP5BB. A copolyester based on PP5BB with 30 mol% bibenzoate replaced with isophthalate (PP5BB-30I) had T_g of 28 °C, close to the PP5BB T_g of 30 °C. Oxygen permeability of PP5BB was 0.0921 compared to 0.314 cc(STP) cm m^{-2} day^{-1} atm^{-1} for PP5BB-30I, Table 2. Lower permeability of PP5BB resulted primarily from lower solubility, 0.0164 compared to 0.0352 cc(STP) cm^{-3} atm^{-1} for PP5BB-30I. A difference in oxygen diffusivity, 6.5×10^{-13} compared to 10.3×10^{-13} m^2 s^{-1} for PP5BB-30I, also contributed to lower permeability of the LCP, although the effect of liquid crystallinity on D was smaller than the effect on S.

Crystallization of PP5BB reduced the oxygen transport parameters as shown in Fig. 10 with crystallinity expressed as density. The lower temperature crystallization reduced P slightly less than the higher temperature crystallization. Decreases in P were due to decreases in both D and S. The linear decrease in S with density extrapolated to $S=0$ at a density of 1.331 g cm^{-3}.

3.7. Two-phase model for oxygen transport

Gas transport in crystalline non-LC polymers is often considered in terms of a two-phase model consisting of an impermeable crystalline phase dispersed in a permeable amorphous matrix [6]. Thus, both sorption and diffusion are seen as taking place in the amorphous phase. The simple two-phase transport model has been extended to smectic PDEGBB by considering impermeable crystals dispersed in a permeable LC glass [6,8]. The resulting relationship between solubility and crystallinity is

$$S = S_{LC}(1-\phi_c) \quad (2)$$

where S_{LC} is the solubility of the gas in the LC glass and ϕ_c is the volume fraction crystallinity. If S_{LC} is independent of the amount of crystallinity and equal to the solubility of the completely glassy LC, S will decrease linearly with volume fraction crystallinity and extrapolate to zero solubility at $\phi_c=1$.

It follows that volume fraction crystallinity ϕ_c can be calculated reliably from density ρ according to

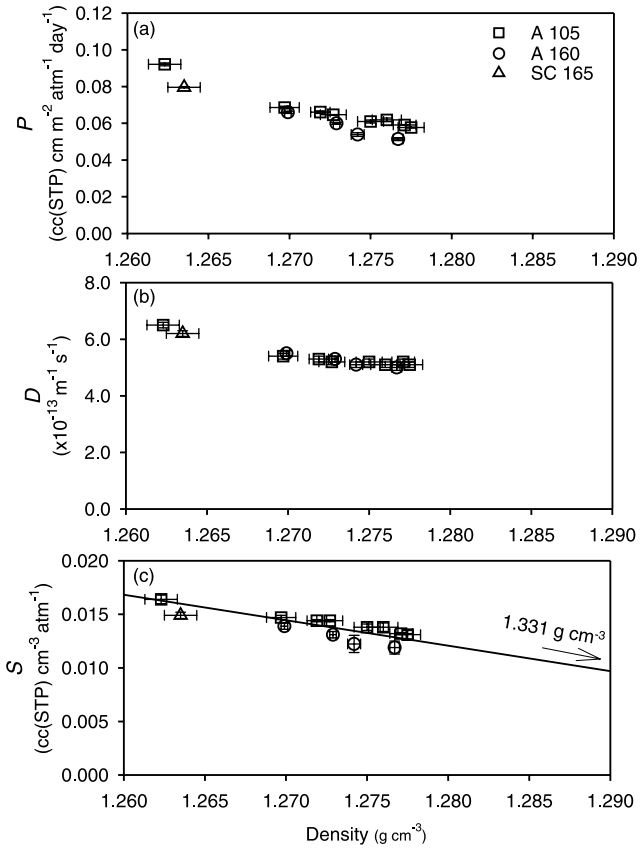

Fig. 10. Effect of crystallinity measured as density on the oxygen transport parameters of PP5BB: (a) permeability; (b) diffusivity; and (c) solubility.

$$\phi_c = \frac{\rho - \rho_{LC}}{\rho_c - \rho_{LC}} \quad (3)$$

where ρ_{LC} and ρ_c are the LC glass and crystal densities, respectively.

In applying Eqs. (2) and (3) to PP5BB the appropriate value for ρ_c is not obvious. The crystal density based on the reported unit cell is 1.377 g cm^{-3} [23]. This value seems too high as it gives unrealistically low values of crystallinity from Eq. (3). Alternatively, the crystal density obtained by extrapolation to zero solubility of $\rho_c = 1.331$ g cm^{-3} may be more reasonable. The group contribution method gives a value of 1.323 g cm^{-3} that is only slightly lower [30]. Moreover, the value of 1.331 g cm^{-3} from solubility is intermediate between the reported crystal density of poly(ethylene 4,4′-bibenzoate) of 1.426 g cm^{-3} [31], and that of poly(hexamethylene 4,4′-bibenzoate) of 1.307 g cm^{-3} [32]. A value of 1.331 g cm^{-3} also seems reasonable when compared with the crystal density of PDEGBB of 1.371 g cm^{-3} [6], considering that the LC glass density of PP5BB is slightly lower than the LC glass density of PDEGBB. Extrapolation of the linear relationship between ΔH_{X-S} and density to 1.331 g cm^{-3} (Fig. 4) yields $\Delta H^0_{X-S} = 75$ J g^{-1} or 23 kJ mol^{-1}. This is consistent with the general observation of low values of ΔH^0 for crystal-to-LC transitions [6,27,33,34].

In conforming to the two-phase transport model, PP5BB confirmed the gas transport model for LCPs established from PDEGBB that considers a liquid crystalline state intermediate between the permeable amorphous glass and the impermeable three-dimensional crystal. In this interpretation, LC order naturally leads to inherently low gas solubility.

The two-phase description of oxygen solubility was taken as the basis for examining diffusivity and permeability of cold-crystallized PP5BB. The decrease in D with crystallinity arises from geometric impedance to the transport path imposed by impermeable three-dimensional crystallites. The result can be dramatic if the effective aspect ratio of the crystallites is large. This occurs in polyesters that crystallize as lamellar crystals organized into spherulitic morphologies such as PET, poly(ethylene naphthalate), and melt-crystallized poly(ethylene terephthalate-*co*-4,4′-bibenzoate) [9–11]. Compared to spherulitic polymers, the effect of crystallization on D of PP5BB is quite modest despite the relatively high level of crystallinity inferred from changes in solubility and density. However, compared to smectic PDEGBB, the effect of crystallization on D is similar. The structural image of crystallized PP5BB is one of small crystallites embedded in LC lamellae. Due to the low aspect ratio, the crystallites impart less tortuosity to the diffusion pathway than lamellar crystallites would.

The concept of crystallized PP5BB as small crystallites of low aspect ratio is modeled as a dispersion of impermeable particles in a permeable matrix. Numerous empirical expressions for permeability of such a dispersion are available, usually with the aspect ratio of the particle as an adjustable parameter. One example is the Nielsen model with permeability expressed as [35]

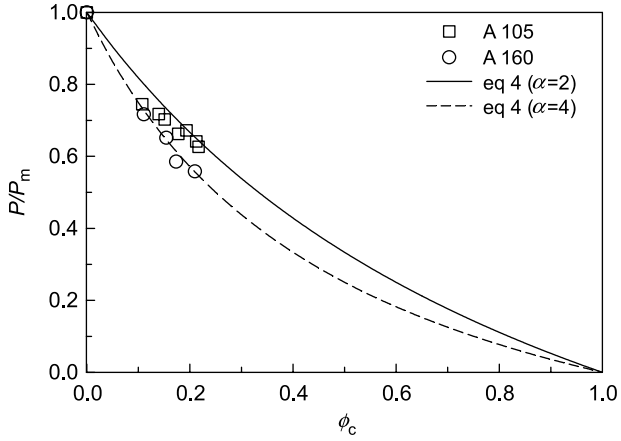

Fig. 11. Relationship between the relative permeability (P/P_m) and ϕ_c for cold-crystallized PP5BB and the fit to the Nielsen model (Eq. (4)).

$$P = P_m \left[\frac{1 - \phi_c}{1 + \alpha/2\phi_c} \right] \quad (4)$$

where P_m is the permeability of the matrix, taken as the permeability of the quenched LC glass of 0.0921 cc(STP) cm m^{-2} day^{-1} atm^{-1}, ϕ_c is the volume fraction crystallinity, and α is the aspect ratio of the dispersed impermeable phase. For $\alpha = 1$, Eq. (4) reduces to the Maxwell equation for impermeable spheres. The quantity P/P_m is plotted versus ϕ_c in Fig. 11. Oxygen permeability for PP5BB cold-crystallized at 105 and 160 °C is well described by Eq. (4) with an aspect ratio of 2–4. Not surprisingly, the higher crystallization temperature yields a slightly better crystal structure as indicated by larger α.

3.8. Comparison between PP5BB with PDEGBB

Both PP5BB and PDEGBB are polyesters of 4,4′-bibenzoic acid and a five-atom diol spacer; the only difference is replacement of the center carbon atom in the pentamethylene spacer of PP5BB with an oxygen atom in PDEGBB. The hierarchical solid state structures correspond closely. Both polymers form the smectic CA type LC glass where the layer normal is parallel to the molecular direction and the mesogenic groups are tilted with respect to the layer normal [6]. Close similarity in molecular organization of the smectic layers is indicated by correspondence in lamellar spacing of 1.54 nm for PP5BB and 1.56 nm for PDEGBB, and appearance of a broad reflection at 20.5° in the WAXD pattern of both polymers which is attributed to spacing of the mesogens. The similarity in hierarchical morphology extends further to stacking of smectic layers into wavy lamellae, although the lamellae of PP5BB tend to be thinner than the lamellae of PDEGBB, and to assembly of lamellae into domains. The domain morphologies produced by the various thermal treatments of PP5BB and PDEGBB are practically identical when viewed by AFM. The lower density of the PP5BB glass, 1.2623 g cm^{-3} compared to 1.3201 g cm^{-3} for the PDEGBB glass, and the larger free volume hole size of PP5BB (Table 2) are attributed to the higher molar volume of the methylene group of

10.23 $cm^3\ mol^{-1}$ compared to the molar volume of the ether oxygen of 5.0–5.5 $cm^3\ mol^{-1}$ [30].

Both PP5BB and PDEGBB undergo cold-crystallization from the LC glass, although the WAXD patterns suggest differences in the unit cell. Nevertheless, in both cases the effect of crystallization supports a simple two-phase gas transport model of impermeable crystallites dispersed in a permeable smectic glass. Due to the low crystallite aspect ratio, crystallization only slightly decreases oxygen diffusivity. This result provides the structural basis for describing oxygen permeability in terms of the Nielsen model for low aspect ratio particles. Despite these similarities, the permeability of PP5BB is about three times higher than that of PDEGBB, Table 2. Higher permeability of PP5BB originates mainly from higher diffusivity compared to PDEGBB. Slightly higher solubility of PP5BB results from the larger free volume hole size.

The surprisingly strong effect of a slight chemical difference on the oxygen diffusivity leads to comparison of other, non-LC aromatic polyesters with pentamethylene diol and diethylene glycol spacers. Replacing 30 mol% of the 4,4′-bibenzoate in PP5BB and PDEGBB with isophthalate (PP5BB-30I and PDEGBB-30I) eliminates the LC character. The oxygen transport characteristics of the non-LC 4,4′-bibenzoate copolymers along with data for some non-LC naphthalate polyesters with pentamethylene diol and diethylene glycol spaces (PP5N and PDEGN) are given in Table 2. The non-LC polyesters with pentamethylene spacers consistently show three-times higher P compared to the corresponding polyesters with diethylene glycol spacers. The difference results mainly from higher D. In addition, pentamethylene polyesters have consistently lower T_g and lower density than the diethylene glycol counterparts.

Diffusivity of the glassy polymer derives from jumps of the gas molecule between free volume holes and depends on conformational changes and segmental motions of the polymer chain. In a glassy polyester, these thermal rearrangements manifest themselves as sub-T_g relaxation processes. Indeed, a relationship between diffusivity and the γ-relaxation intensity, particularly the relaxation component associated with gauche conformations of the glycol, was demonstrated previously for PET and copolymers based on PET [36,37]. Therefore, an explanation for the low D of polymers with the diethylene glycol spacer compared to the pentamethylene spacer was sought in the secondary relaxation behavior.

The γ-relaxation of polyterephthalates and polyisophthalates with up to 10 methylene units in the spacer is reported to consist of two overlapping processes associated with gauche and trans conformations, respectively [38]. The effect of increasing the number of carbon atoms in the spacer is an overall shift to lower temperatures and an increase in the relative intensity of the lower temperature component [39]. The two components of the γ-relaxation are clearly resolved in the relaxation spectrum of PP5BB (Fig. 6). Although the conformations of the oxymethylene chain are thought to differ significantly from those of the all-methylene chain, molecular mechanics calculations suggest that oxygen atoms actively participate in restricted motions that give rise to the γ-relaxation of polybibenzoates with oxyethylene spacers [40].

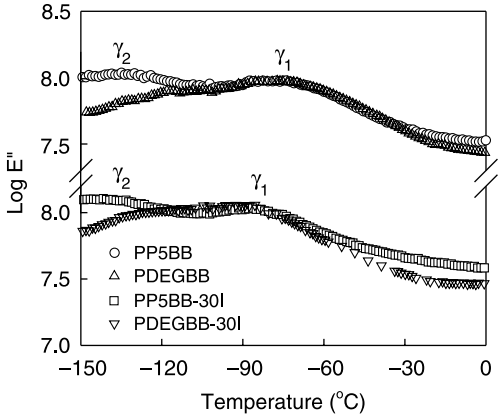

Fig. 12. Temperature dependence of log E'' in the γ-relaxation region for quenched PP5BB, PP5BB-30I, PDEGBB and PDEGBB-30I.

Relaxation behavior of PP5BB, PDEGBB, PP5BB-30I and PDEGBB-30I is reported as loss modulus in Fig. 12. The results for PP5BB and PDEGBB confirm previous reports of two components in the broad relaxation peak [40]. The primary difference between the two types of spacers is the lower intensity of the γ_2 component for the diethylene glycol spacers. Considerably lower relaxation intensity in this region suggests that gauche conformations of the diethylene glycol spacer are less numerous, which is consistent with higher trans fraction (Table 2), and/or gauche conformations have lower mobility. From the general relationship between diffusivity and the γ-relaxation intensity, particularly the relaxation component associated with gauche conformations of the glycol, it follows that the significantly lower γ_2 intensity is responsible for the lower diffusivity of polyesters with diethylene glycol spacers.

4. Conclusions

This study extends the model for oxygen transport of smectic LC polyesters based on bibenzoate. Like the previously studied poly(diethylene glycol 4,4′-bibenzoate), the solid state structure of poly(pentamethylene 4,4′-bibenzoate) can be varied systematically from the LC glass to the crystallized LC glass. Results for oxygen transport are consistent with a glassy liquid crystalline state intermediate between the permeable amorphous glass and the impermeable three-dimensional crystal. Crystallized PP5BB is amenable to a simple two-phase transport model consisting of an impermeable crystalline phase dispersed in a permeable LC glass. The hierarchical structure of the crystallized LC glass provides the basis for describing the relatively small effect of crystallinity in terms of the Nielsen permeability model for a dispersion of low aspect ratio particles.

Furthermore, the study compares the effect of replacing the center methylene group in the pentamethylene spacer with an ether oxygen. Oxygen permeability of LC and non-LC diethylene glycol polyesters is three times lower than that of the corresponding pentamethylene polyesters, primarily due to

reduced diffusivity. The origin of lower diffusivity is found in the γ-relaxation behavior. The results extend our understanding of the relationship between diffusivity and the γ-relaxation intensity, particularly the relaxation component associated with gauche conformations of the glycol, that was developed previously for PET and copolymers based on PET.

Acknowledgements

The authors thank Prof D.A. Schiraldi for assistance in obtaining the polymers and Dr R.Y.F. Liu for providing the infrared determination of trans conformation fraction. Modern Controls, Inc., is thanked for generous support of the facility for gas transport studies at Case Western Reserve University.

References

[1] Chiou JS, Paul DR. J Polym Sci, Part B: Polym Phys 1987;25:1699–707.
[2] Weinkauf DH, Paul DR. J Polym Sci, Part B: Polym Phys 1991;29: 329–40.
[3] Weinkauf DH, Paul DR. J Polym Sci, Part B: Polym Phys 1992;30: 837–49.
[4] Weinkauf DH, Paul DR. In: Koros WJ, editor. Barrier polymers and structures. Washington DC: American Chemical Society; 1990. p. 60–91 [chapter 3].
[5] Weinkauf DH, Paul DR. J Polym Sci, Part B: Polym Phys 1992;30: 817–35.
[6] Hu YS, Schiraldi DA, Hiltner A, Baer E. Macromolecules 2003;36: 3606–15.
[7] Hu YS, Liu RYF, Schiraldi DA, Hiltner A, Baer E. Macromolecules 2004; 37:2128–35.
[8] Hu YS, Liu RYF, Schiraldi DA, Hiltner A, Baer E. Macromolecules 2004; 37:2136–43.
[9] Sekelik DJ, Stepanov SV, Nazarenko S, Schiraldi D, Hiltner A, Baer E. J Polym Sci, Part B: Polym Phys 1999;37:847–57.
[10] Hu YS, Liu RYF, Zhang LQ, Rogunova M, Schiraldi DA, Nazarenko S, et al. Macromolecules 2002;35:7326–37.
[11] Hu YS, Liu RYF, Rogunova M, Schiraldi DA, Nazarenko S, Hiltner A, et al. J Polym Sci, Part B: Polym Phys 2002;40:2489–503.
[12] Krigbaum WR, Asrar J, Toriumi H, Ciferri A, Preston J. J Polym Sci, Polym Lett Ed 1982;20:109–15.
[13] Meurisse P, Noel C, Monnerie L, Fayolle B. Br Polym J 1981;13:55–63.
[14] Watanabe J, Hayashi M, Nakata T, Niori T, Tokita M. Prog Polym Sci 1997;22:1053–87.
[15] Higuchi H, Yu Z, Jamieson AM, Simha R, McGervey JD. J Polym Sci, Part B: Polym Phys 1995;33:2295–305.
[16] Qureshi N, Stepanov EV, Schiraldi D, Hiltner A, Baer E. J Polym Sci, Part B: Polym Phys 2000;38:1679–86.
[17] Organ SJ, Barham PJ. Polym Prepr 1988;29:602.
[18] Watanabe J, Hayashi M. Macromolecules 1988;21:278–80.
[19] Tokita M, Osada K, Watanabe J. Polym J 1998;30:589–95.
[20] Bello A, Riande E, Pérez E, Marugán MM, Pereña JM. Macromolecules 1993;26:1072–7.
[21] Watanabe J, Hayashi M. Macromolecules 1989;22:4083–8.
[22] Tokita M, Osada K, Watanabe J. Liq Cryst 1998;24:477–80.
[23] Osada K, Niwano H, Tokita M, Kawauchi S, Watanabe J. Macromolecules 2000;33:7420–5.
[24] Hu YS, Rogunova M, Schiraldi DA, Hiltner A, Baer E. J Appl Polym Sci 2002;86:98–115.
[25] Thomas EL, Wood BA. Faraday Discuss Chem Soc 1985;79:229–39.
[26] Butzbach GD, Wendorff JH, Zimmermann HJ. Polymer 1986;27: 1337–44.
[27] Grebowicz J, Wunderlich B. J Polym Sci, Polym Phys Ed 1983;21: 141–50.
[28] Hudson SD, Lovinger AZ, Gomez MA, Jorente J, Marco C, Fatou JG. Macromolecules 1994;27:3357–62.
[29] Pérez E, Benavente R, Bello A, Pereña JM, VanderHart DL. Macromolecules 1995;28:6211–8.
[30] Van Krevelen DW. Properties of polymers. 3rd ed. Amsterdam: Elsevier; 1997 [chapter 4, p. 71–107].
[31] Li X, Brisse F. Macromolecules 1994;27:2276–82.
[32] Li X, Brisse F. Macromolecules 1994;27:7725–34.
[33] Campoy I, Marco C, Gómez MA, Fatou JG. Macromolecules 1992;25: 4392–8.
[34] Cheng SZD. Macromolecules 1988;21:2475–84.
[35] Nielsen LE. J Macromol Sci 1967;A1:929–42.
[36] Polyakova A, Liu RYF, Schiraldi DA, Hiltner A, Baer E. J Polym Sci, Part B: Polym Phys 2001;39:1889–99.
[37] Andrade GS, Collard DM, Schiraldi DA, Hu YS, Baer E, Hiltner A. J Appl Polym Sci 2003;89:934–42.
[38] Yip HK, Williams HL. J Appl Polym Sci 1976;20:1217–30.
[39] Uralil F, Sederel W, Anderson JM, Hiltner A. Polymer 1979;20:51–4.
[40] Heaton NJ, Benavente R, Pérez E, Bello A, Pereña JM. Polymer 1996;37: 3791–8.